NASA/CR-2008-215542

Development and Evaluation of Sensor Concepts for Ageless Aerospace Vehicles

Report 4 – Phase 1 Implementation of the Concept Demonstrator

David Abbott, Adam Batten, David Carpenter, John Dunlop, Graeme Edwards, Tony Farmer, Bruce Gaffney, Mark Hedley, Nigel Hoschke, Peter Isaacs, Mark Johnson, Chris Lewis, Alex Murdoch, Geoff Poulton, Don Price, Mikhail Prokopenko, David Rees, Andrew Scott, Sarath Seneviratne, Philip Valencia, Peter Wang, Denis Whitnall
CSIRO Telecommunications & Industrial Physics, Lindfield, New South Wales, Australia

November 2008

The NASA STI Program Office . . . in Profile

Since its founding, NASA has been dedicated to the advancement of aeronautics and space science. The NASA Scientific and Technical Information (STI) Program Office plays a key part in helping NASA maintain this important role.

The NASA STI Program Office is operated by Langley Research Center, the lead center for NASA's scientific and technical information. The NASA STI Program Office provides access to the NASA STI Database, the largest collection of aeronautical and space science STI in the world. The Program Office is also NASA's institutional mechanism for disseminating the results of its research and development activities. These results are published by NASA in the NASA STI Report Series, which includes the following report types:

- TECHNICAL PUBLICATION. Reports of completed research or a major significant phase of research that present the results of NASA programs and include extensive data or theoretical analysis. Includes compilations of significant scientific and technical data and information deemed to be of continuing reference value. NASA counterpart of peer-reviewed formal professional papers, but having less stringent limitations on manuscript length and extent of graphic presentations.

- TECHNICAL MEMORANDUM. Scientific and technical findings that are preliminary or of specialized interest, e.g., quick release reports, working papers, and bibliographies that contain minimal annotation. Does not contain extensive analysis.

- CONTRACTOR REPORT. Scientific and technical findings by NASA-sponsored contractors and grantees.

- CONFERENCE PUBLICATION. Collected papers from scientific and technical conferences, symposia, seminars, or other meetings sponsored or co-sponsored by NASA.

- SPECIAL PUBLICATION. Scientific, technical, or historical information from NASA programs, projects, and missions, often concerned with subjects having substantial public interest.

- TECHNICAL TRANSLATION. English-language translations of foreign scientific and technical material pertinent to NASA's mission.

Specialized services that complement the STI Program Office's diverse offerings include creating custom thesauri, building customized databases, organizing and publishing research results ... even providing videos.

For more information about the NASA STI Program Office, see the following:

- Access the NASA STI Program Home Page at ***http://www.sti.nasa.gov***

- E-mail your question via the Internet to help@sti.nasa.gov

- Fax your question to the NASA STI Help Desk at (301) 621-0134

- Phone the NASA STI Help Desk at (301) 621-0390

- Write to:
  NASA STI Help Desk
  NASA Center for AeroSpace Information
  7115 Standard Drive
  Hanover, MD 21076-1320

NASA/CR-2008-215542

Development and Evaluation of Sensor Concepts for Ageless Aerospace Vehicles

Report 4 – Phase 1 Implementation of the Concept Demonstrator

David Abbott, Adam Batten, David Carpenter, John Dunlop, Graeme Edwards, Tony Farmer, Bruce Gaffney, Mark Hedley, Nigel Hoschke, Peter Isaacs, Mark Johnson, Chris Lewis, Alex Murdoch, Geoff Poulton, Don Price, Mikhail Prokopenko, David Rees, Andrew Scott, Sarath Seneviratne, Philip Valencia, Peter Wang, Denis Whitnall
CSIRO Telecommunications & Industrial Physics, Lindfield, New South Wales, Australia

National Aeronautics and
Space Administration

Langley Research Center
Hampton, Virginia 23681-2199

Prepared for Langley Research Center
under Purchase Order L-71346D

November 2008

The use of trademarks or names of manufacturers in this report is for accurate reporting and does not constitute an official endorsement, either expressed or implied, of such products or manufacturers by the National Aeronautics and Space Administration.

Available from:

NASA Center for AeroSpace Information (CASI)
7115 Standard Drive
Hanover, MD 21076-1320
(301) 621-0390

National Technical Information Service (NTIS)
5285 Port Royal Road
Springfield, VA 22161-2171
(703) 605-6000

Table of Contents

1. Introduction

NASA's goal of ageless or robust aerospace vehicles (RAVs) requires the development of vehicles that are capable of structural self-assessment and repair. This project is concerned primarily with the self-assessment, or health monitoring, functions at this stage, but it will progress towards the incorporation of damage prognostics to enable intelligent, forward-looking damage mitigation decisions to be made. The health monitoring functions can be divided between those carried out by distributed sensors and intelligent processing and communication on the skin or within the structure, and those that could be more effectively provided by autonomous robotic NDE agents which could be deployed to monitor damage or integrity of the vehicle structure.

Critical to the success of the Ageless Vehicle program are the development of appropriate technologies for non-destructive evaluation of structures, and the development of strategies and technologies for processing NDE data, storage and communication of NDE information, and analysis of NDE data with capability for intelligent decision-making.

Previous work in this project developed and examined concepts for integrated smart sensing and communication systems that could form the distributed sensing function of a smart vehicle. This work was outlined in three earlier Reports (CTIP, 2001; CTIP, 2002; CTIP, 2003). The third of these Reports (CTIP, 2003) contained a proposal for the design of a Concept Demonstrator and Experimental Test-bed: a combined hardware and software system capable of demonstrating principles of an intelligent vehicle health monitoring system. The first stage of the development of this Concept Demonstrator (CD) is now complete, and this Report contains a brief outline of some of its features and capabilities.

Details of the purpose and design of the CD were presented in our last Report (CTIP, 2003), and they will not be repeated here. However, there have been some modifications to the original plans. Initial construction of the CD has been a substantially greater engineering task than was anticipated when the original contract schedule was agreed, and it has not been possible to complete the electronic design and construction in the time available.

Therefore, with the approval of NASA, a version of the CD that is incomplete but which nevertheless demonstrates all of the essential functionality of the complete system, has been developed. It has only a small number of fully functional sensing cells: 16 cells in a 4×4 array have functional Network Applications Sub-modules, the electronic sub-systems that control the network communications, and 5 of these have sensors and Data Acquisition Sub-modules, which acquire and pre-process the sensor data. These 16 cells will be referred to as physical cells. However, in addition to this, a number of cells (3 arrays of 4×4 cells) have been simulated in Personal Computers, with each cell running as a separate process, and each 4×4 array in a separate PC. These will be referred to as simulated cells. The 16 physical cells and 48 simulated cells are connected together to form a single 8×8 array. Further details of this hybrid system are given below.

While development of the hybrid system was a response to a shortage of development time, it has had at least one very positive outcome. The need to include both digital signal processor (DSP)-based and Personal Computer (PC)-based agents in a single network has

meant that some problems involved in implementing a heterogeneous network (e.g. processor timing differences, hardware interface differences, etc.) have been addressed and solved. This would not have been the case if a homogeneous network of agents had been implemented as originally planned.

The purpose of the CD is to demonstrate concepts for an intelligent vehicle health monitoring system within a relatively simple environment. It was decided that, at least in the first instance, the only threats to the structure that would be considered would be from impacts by projectiles that, for a vehicle in space, might be micrometeoroids or space debris. A summary of threats associated with particle impacts, compiled from a number of sources, appears in Report 2 (CTIP (2002), Section 5.3 and Appendix A5.1). *Thus, the aim of the initial design of the CD is only to enable the detection, location and evaluation of the effects of particle impacts.* It is expected that other threats and damage processes will be addressed in later stages of the project.

One of the most important principles of the design, and one that distinguishes a health monitoring system from other intelligent sensing systems (or "smart spaces"), is the requirement for continued functionality in the presence of damage. A system designed to detect and evaluate damage, and ultimately initiate repair and/or other remedial action, clearly must continue to operate effectively when damage occurs, whether it is damage to the vehicle structure, damage to the sensing system, or both.

The remainder of this Report is set out as follows. The next Section contains a general overview of the CD system in its present form. This is followed by a description of the sensor development and testing, using both high-velocity particles and laser pulses. Then follow Sections that outline the structure and performance of the physical cells (Section 4) and simulated cells (Section 5), the system management workstation and visualizer (Section 6), an outline of the intelligent agent software that has been implemented in the system (Section 7), followed by a brief summary and conclusions.

Finally, it should be emphasized that this structure is intended purely as a test-bed and demonstrator for concepts and techniques, and is not intended to represent a realistic prototype system. It has been designed to provide a high level of processing power to allow maximum flexibility, with little consideration given to weight, complexity or power consumption (all of which will be major issues in practical systems). Cost has, of course, been a factor, but not to the extent it would be in most practical applications.

2. System Overview

2.1 Introduction

The initial goal of the present CD system is the detection and characterization of high-velocity impacts, such as might be caused by micrometeoroids in space. Passive piezo-polymer sensors have been bonded to the inside surface of the vehicle 'skin', with an average distance between sensors of about 50 mm, to detect the elastic waves generated in the structure by impacts. The sensors, processing and communications hardware are constructed as modules, each of which contains a group of sensors on a 100 mm × 100 mm area of the aluminium sheet skin, with the electronics being mounted in layers directly behind the sensors. This unit is termed a 'cell'. A schematic diagram of the system is given in Figure 1.

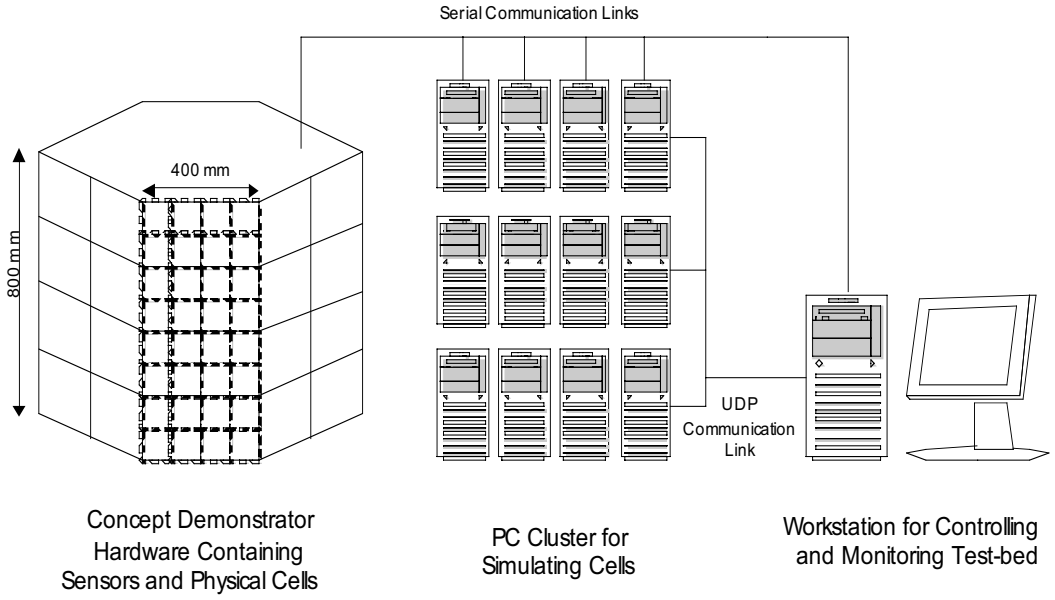

Figure 1: Schematic diagram of the test-bed, showing the physical structure and cells, simulated cells, and test-bed control workstation. Each side of the concept demonstrator hexagonal structure is divided into 4 × 2 Panels, each of which contains 2 × 2 Cells, which are the basic modular units for construction.

2.2 Physical Structure

The structure of the concept demonstrator is a hexagonal prism, with each rectangular face being 400 mm × 800 mm. A modular aluminium frame is covered by 200 mm square, 1 mm thick aluminium panels that form the outer skin of the structure. Each such panel contains four cells, and each of the six sides of the prism contains eight of these panels, so the entire concept demonstrator contains 48 panels and 192 cells (see Figure 1). As each cell contains four sensors there are a total of 768 piezo-polymer sensors in the initial system.

This structure has been placed on a platform that enables it to be rotated and elevated, which simplifies testing as it is easier to move the structure than the source of high-velocity particles (to be described later). As the design has been modularized, the same hardware could be readily applied to a different structure if desired.

Although the initial system uses a single type of sensor to measure a single threat, namely high-velocity impacts, the system has been designed so that in the near future the concept demonstrator may be extended to use multiple sensor types to detect and characterize a range of threats.

2.3 Modules and Layers

A modular approach to the sensing and electronics was adopted to enhance flexibility, re-configurability and ease of manufacture (see Hedley et al., 2003 for more details). Each module, or cell, contains sensing elements, signal processing (analog and digital) and communications, and there is a logical layering of these functions, as follows.

1. Sensors – initially piezo-polymer sensors only are attached to the aluminium skin.
2. Analog signal processing – this includes amplification, filtering and other processing of the sensor signals required prior to digitization of the signals.
3. Sampling and data pre-processing – this includes digitization, calibration correction, data reduction and other processing that can be performed using only the local signals.
4. Data analysis – at this level data is processed using information from local sensors and neighbouring modules. This is the layer at which the agent-based algorithms will be implemented to provide the network intelligence.
5. Inter-module communication – this layer comprises the software stack and the physical links to provide communication between modules.

These layers are divided into two groups, the Data Acquisition Layer (DAL), which consists of layers 1 to 3, and the Network Application Layer (NAL), which consists of layers 4 and 5. These groups are implemented as separate physical sub-modules, called the Data Acquisition Sub-module (DAS) and Network Application Sub-module (NAS) respectively. This is illustrated in Figure 2. This separation allows replacement of one type of sensor, and its associated electronics, with another sensor sub-module, without changing the main processing and communications hardware, hence simplifying the use of a range of sensor types in the test-bed. There are separate digital signal processors (DSPs) in each sub-module, and these are called the Data Acquisition Processor (DAP) and Network Application Processor (NAP) respectively.

Each DAL sub-module communicates with one NAL sub-module, and network communication is provided by each NAL sub-module communicating with its four nearest neighbours. This provides a highly robust mesh network structure that will maintain connectivity even when a significant number of cells or communications links are damaged.

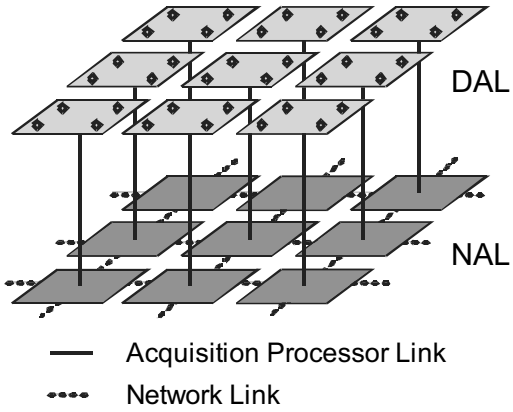

Figure 2: Layer structure and communications of the cells. Each cell contains a Data Acquisition Sub-module (DAS), which collectively form the DAL, and a Network Application Sub-module (NAS), with communications links between the Network Application Sub-modules forming a mesh network structure (the NAL).

3. Sensor Development and Testing

3.1 Introduction

Report 3 (CTIP, 2003) outlined a possible design of an integrated impact sensor using PVDF sheet, that included a large-area sensor (about 90 mm square) and four smaller sensors (2.5 mm diameter) within this area. These sensors detected satisfactorily the simulated 'impacts' using pulses from a Q-switched laser. While a number of potential problems with the large-area sensor were flagged (EMI susceptibility and low signal-to-noise ratios, mainly due to its large capacitance), the sensors had not yet been tested using fast particle impacts. Aluminium panels 1 mm thick, complete with four integrated sensors bonded to one side, were fabricated using techniques outlined in earlier reports. The electrode pattern on the PVDF was silk-screen printed, a technique that allowed the manufacture of many sheets, all essentially identical.

3.2 High-velocity impact experiments

A free-piston shock tube at the Centre for Hypersonics, University of Queensland, was modified to function as a light-gas gun. It was capable of accelerating 1-mm diameter stainless steel balls to velocities up to about 1.5 km/s. The velocity of the projectile could be varied by changing the compression tube pressure, reservoir pressure and blast tank pressure. The way the shock tube had been modified and the distance from the end of the launch tube to the target gave rise to a reasonable variation in both the projectile's speed and its impact site position. In order to simplify the gun operation only two sets of pressure conditions were used to generate two sets of projectile speeds in the regions of 200 m/s and 1000 m/s. (For a 1-mm diameter stainless steel ball, with mass 4 mg, these speeds correspond to kinetic energies of 0.08 J and 2 J respectively.) A three-beam laser system was set up to measure the velocity of the particles, but because of the trajectory variation not all shots were detected by this system.

3.3 Experimental set-up

The projectiles were incident on an aluminium sheet mounted in the blast tank, which could be evacuated. On the rear side of the sheet were epoxy-bonded four integrated sensors, each one consisting of a large-area sensor and four small-area sensors. Connections to the sensors were made via spring-loaded pins, held in position by a piece of printed circuit board, mounted on an aluminium bar that in turn was mounted to the aluminium sheet. Oscilloscope probes were connected to the pins and coupled out of the blast tank through a plate with multiple BNC feed-throughs. A similar arrangement has been used whilst monitoring signals from plates mounted on the concept demonstrator itself.

Signals from all four small-area sensors and the large-area sensor were monitored, as well the large-area and a small-area sensor of a neighbouring integrated sensor. For most of the experiments particles were aimed at and hit the panels at normal incidence, but in a few the effects of oblique incidence were studied by mounting the sheet at 45 to the incoming projectiles. Some shots were also fired into 2 mm thick sheets of aluminium. A total of 38 shots were recorded.

After completion of the particle impact tests, some of the panels used in the gas gun experiments were subjected to laser pulse 'impacts' near the site of the particle impacts. This allowed an almost direct comparison of the signal characteristics from the sensors subjected to the elastic waves generated by these two very different sources of energy. Laser 'impacts' were made within about 10 mm of the site of the particle impact.

3.4 Results

Fast particle impacts

Figure 3 shows the large- and small-area sensor signals from low- and high-velocity particle impacts. As in the case of the laser results described in Report 3, it is clear from the particle-impact experiments that the flexural wave (A_0) signal gives rise to the largest signal amplitude from the small-area sensors. Both the flexural wave (A_0) and the extensional wave (S_0) signals, but particularly the latter, show the presence of more high-frequency components in the higher velocity results. This may be due to the shorter interaction time of the high-velocity particle with the skin. It will clearly be important to distinguish impacts that pierce the skin from those that do not. The possibility of using the S_0 spectrum to do this is being investigated.

While the signals from the small-area sensors during the impact experiments looked similar (in shape if not amplitude) to those generated in the preliminary laser 'impact' experiments described in Report 3 (CTIP, 2003), the signals from the large-area sensors were very different. Laser-generated elastic waves gave rise to short-duration pulses in the large-area sensor signals, separated by the reverberation time through the thickness of the aluminium sheet, thus providing a suitable trigger signal for monitoring the other sensor signals. The two large-area signals from the particle impacts show no such pattern (Figure 3). In general it can be said that these signals slowly deviated from zero as the projectile impacted the aluminium sheet. The initial change in the signal takes a few microseconds, followed by a slowly rising signal over tens of microseconds. This behaviour has been tentatively ascribed to the deceleration of the steel ball in the aluminium sheet (a steel ball travelling at 1 km/s will take about 2 μs to uniformly decelerate to a halt over a distance of 1 mm), followed by flexure and the subsequent plate waves in the aluminium sheet. This deceleration time, coupled with the fact that the sheet is being significantly distorted by the impacting particle, will wash out all the reverberation effects that are so pronounced when using the fast, surface excitation provided by the laser. Thus the large-area sensor, when impacted with particles at these velocities, does not provide a large, sharp signal to trigger further data acquisition processes.

Further, little correlation was found between the signal characteristics of the large-area sensors and the severity of damage. The variability in the signals may be explained, at least in part, by the different ways the PVDF film can break when the aluminium is penetrated: it can distort but not break, it can split along the 'grain' (or stretching direction) of the PVDF, or it can be shredded.

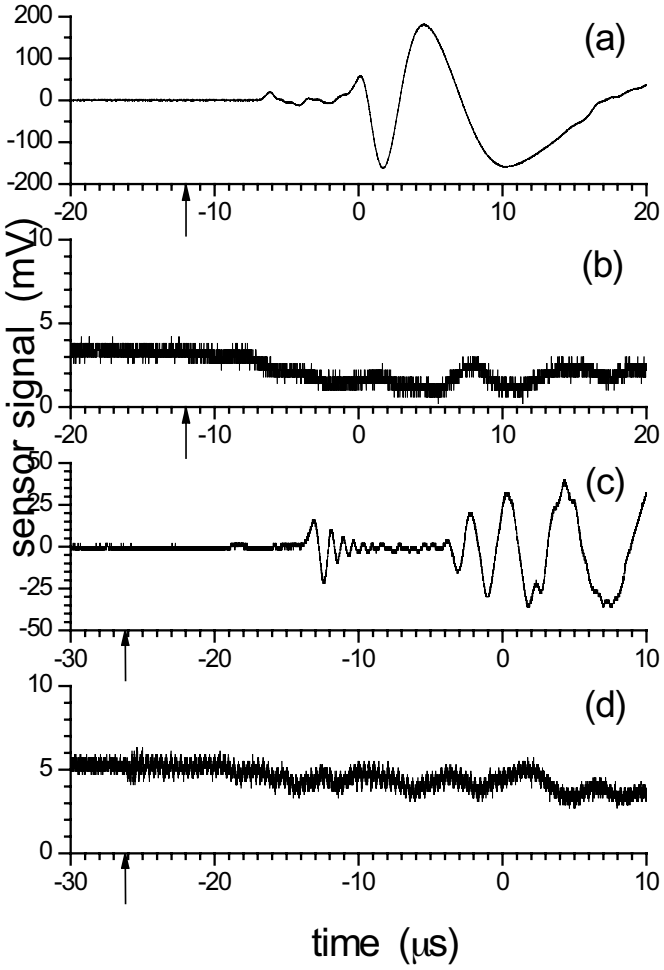

Figure 3: (a) Small-area sensor signal from a low-velocity impact, 200 m/s. (b) Large-area sensor signal from the same low-velocity impact, 200 m/s. (c) Small-area sensor signal from a high-velocity impact, 1 km/s. (d) Large-area sensor signal from the same high-velocity impact, 1 km/s. The arrows show the time of impact.

Neighbouring large-area sensors always registered a signal, but one that was lower in amplitude than that from the large-area sensor that is struck. Finally, the large-area signals were always significantly smaller in amplitude than the small-area sensor signals, by one or two orders of magnitude. This is primarily a consequence of the capacitance of the film and the effects of phase cancellation.

The very different nature of the large-area sensor signal from real impacts as opposed to the laser pulses, indicates that at this stage it is not worth using the large-area sensor for the purpose for which it was designed, namely to monitor a large area of the concept demonstrator's surface, and initiate on impact the acquisition of more detailed data from the small-area sensors. Other aspects, such as the large capacitance of the sensor and hence its reduced signal-to-noise ratio compared with the small-area sensors, the difficulty of electrically shielding the sensor, and the challenges of achieving uniform, repeatable

bonding over a large area have also contributed to the decision to use only small-area sensors at this stage.

Results from the 45 impacts and the 2 mm aluminium sheet did not indicate any significant differences in the sensor signals to the normal-incidence results on 1-mm thick aluminium sheet.

Comparison of laser and particle impacts

The output of a Q-switched Nd:YAG laser was used (as described in Report 3 (CTIP, 2003)) to simulate impacts on the same sensors and aluminium sheets used in the particle impact experiments. The laser was focused to points near to the original particle impact sites.

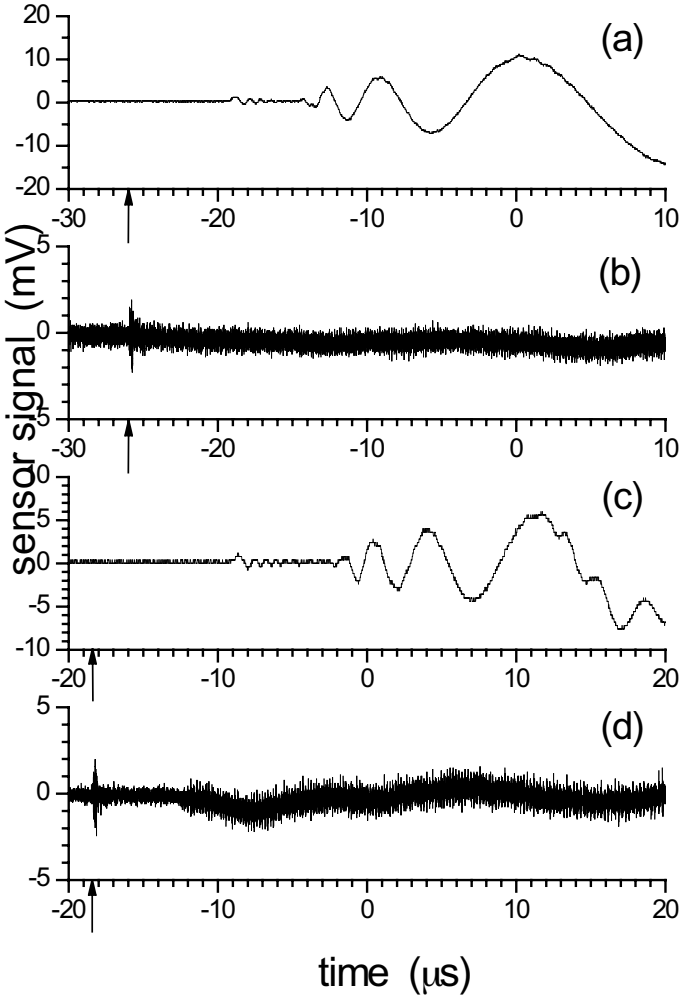

Figure 4: (a) Small-area sensor signal from a laser 'impact', near the site of the particle impact of Fig. 3(a). (b) Large-area sensor signal from the same laser 'impact'. (c) Small-area sensor signal from the laser 'impact' near the site of the particle impact of Fig. 3(c). (d) The large-area sensor signal from the same laser 'impact'. The arrows show the time of impact.

Figure 4 shows the signals obtained from the sensors when the laser pulse was used as the 'impact' near the particle impact sites corresponding to the results in Figure 3. The laser pulses used were 8 ns FWHM with pulse energy of 0.5 J. The total amount of energy that is converted into elastic waves in the material has not been calculated, but such a calculation would need to account for the various effects of reflection, scattering, absorption, surface roughening, plasma shielding, heating and any other processes parasitic to the delivery of energy. Clearly the signals obtained from the laser 'impacts' are significantly lower in amplitude than those obtained from particle impacts. A complete comparison of all the signals has not been undertaken, although it appears that the factor by which the particle impact signals are larger than the laser-generated signals is about 15 for the extensional wave signals and about 5 for the flexural wave signals (looking at the maximum amplitudes that occurred during the measurement period). These factors do not depend significantly on the particle impact velocity.

On the other hand, the particle impact results indicate that the amplitudes of the elastic waves appear to decrease as the reciprocal of the distance from the impact site, so the energy of the waves would go as the square of this quantity. This is a faster decrease than is expected to result from beam-spreading alone (energy density $\propto 1/r$), but perhaps attenuation is playing a role.

In the case of the low-velocity impact signals, it is clear that the laser-generated signals exhibited a larger bandwidth than the impact-generated signals, which is especially evident in the S_0 Lamb wave signals. In the high-velocity case the bandwidths of the laser and particle signals are comparable. While a detailed comparison of the laser- and particle-impact signals would be interesting, it is not believed to be particularly germane to the present project.

The important point is that if only the small-area sensors are to be used at this stage of the project then elastic waves generated by the laser may be used to test the sensing and processing systems responses, as they display most of the features of the signals from particle impacts, despite the remarkably dissimilar generation mechanisms. Using a laser is quicker and easier than using a gas gun. It will always be borne in mind that at each stage of the development of the concept demonstrator crucial design elements will need to be checked by subjecting the demonstrator to real impacts.

3.5 Signal processing

For subsequent experiments, for testing the data processing hardware and communications and simulation software, a number of panels have been made that have only small-area sensors attached. PVDF patches of 10 mm diameter were epoxy-bonded to the aluminium sheets and a 2.5-mm diameter electrode of conductive paint applied to its centre. This active area was chosen as a compromise between having a spot large enough to allow easy and reliable positioning of the electrodes to mate with the spring-loaded pins held in a printed circuit board, and not so large as to cause phase cancellation of the waves of interest, increase the capacitance of the sensor, or reduce the precision with which triangulation may be carried out.

For the purposes of testing the first version of the signal processing and intelligent software of the concept demonstrator, it was decided that the extensional wave signal would be used to determine the location and, very roughly, the energy imparted to the skin by the impact. This may be done by measuring the arrival time of the fastest extensional wave mode (at low frequency) and the maximum amplitude of this low-frequency component. In order to facilitate this measurement, the signal from the each of the small-area sensors is buffered, filtered to pass only frequencies above 500 kHz, amplified, and further filtered to pass only frequencies below 1.5 MHz. This band-pass filtering rids the signal of all the low-frequency reverberations around the aluminium plate, and all the high-frequency EMI from the laser, and more importantly is necessary to retain only signal components below the Nyquist frequency corresponding to the 3 MHz sampling rate of the present processors. This signal conditioning is carried out on the PC board that holds the spring-loaded pins that connect to the small-area sensors. There are eight extra pins around the periphery of the PCB that bear upon the earthed sheet of aluminium to reduce any earth-loop problems. Photographs of the signal conditioning and data acquisition boards are shown in Figure 5.

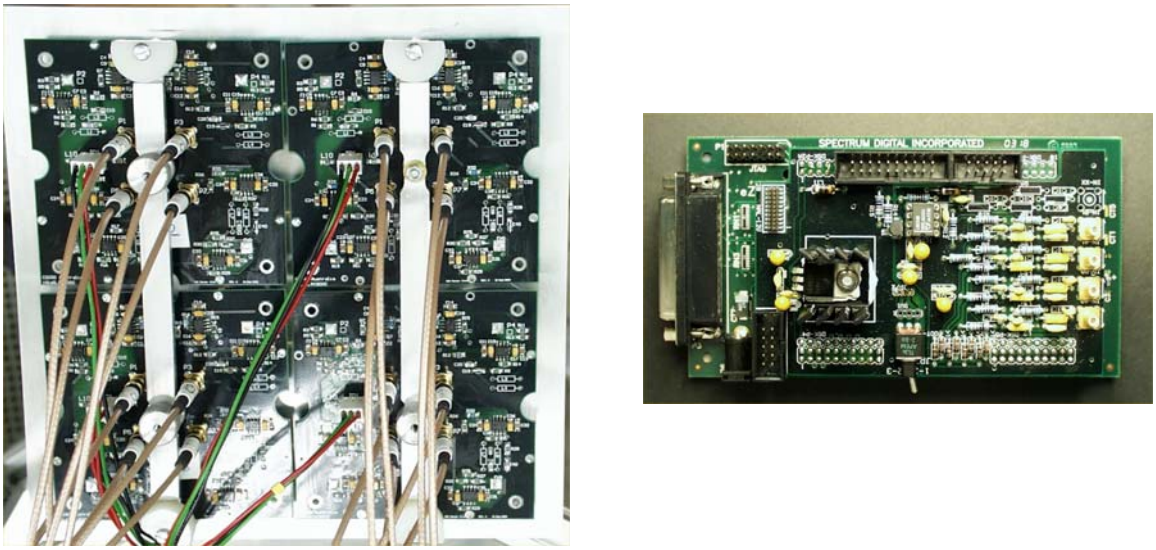

Figure 5: Photographs of the four signal conditioning boards mounted on a sensing panel (left), and one of the prototype data acquisition sub-modules (right).

Figure 6 shows the signals measured at various stages of conditioning. The figure shows, from top to bottom, the raw signal from the sensor, the signal after the high-pass filter, and the signal following the low-pass filter. This sequence of signals clearly shows how the extensional wave component is amplified and cleaned for easy processing. In the final signal, reflections from the edge of the plate of both the extensional and flexural waves can be seen.

The same data is reproduced on a longer timescale in Figure 7. This demonstrates that the amplification, and particularly the filtering, reduces the ‘dead-time’ of the sensor from about 5 ms to about 1 ms, thereby increasing by a factor of five the capability of the system to respond to impacts (from 200 impacts per second to 1000 impacts per second).

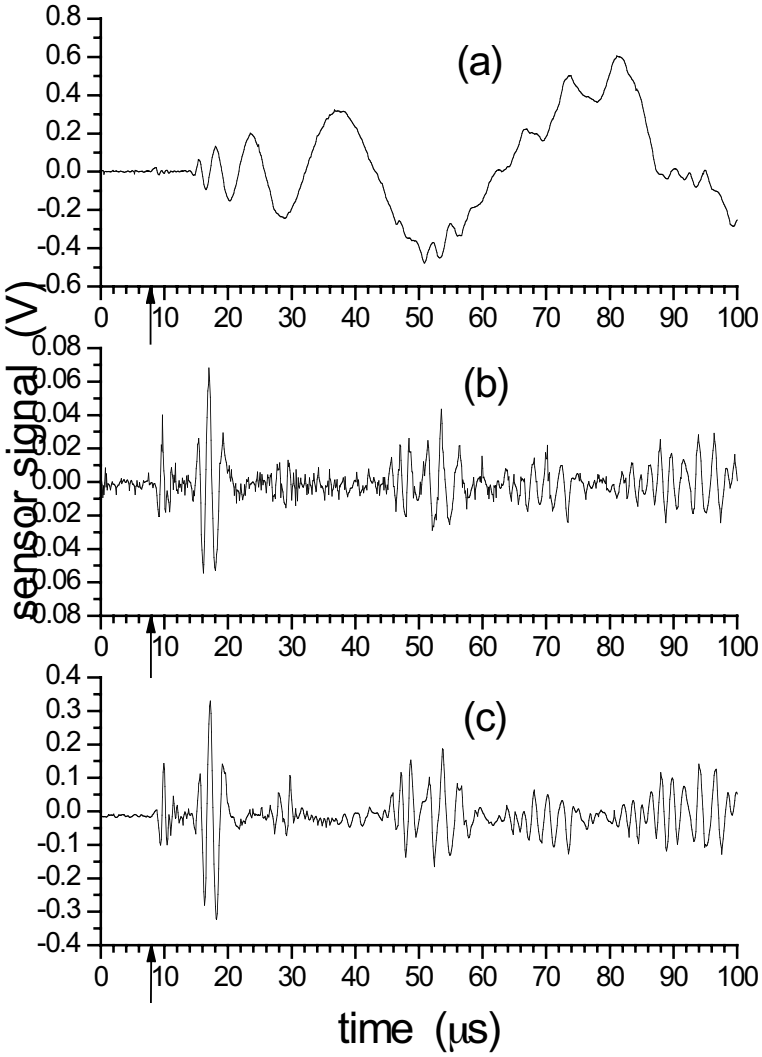

Figure 6: Signal from a small-area sensor monitoring a laser-generated impact. (a) Raw signal. (b) Signal after high-pass filtering. (c) Signal after amplification and low-pass filtering. The arrows show the time of impact.

The conditioned signals from sets of four small-area sensors are then digitized with a sampling interval of 320 ns and stored in a rolling buffer. When any of the four signals deviates from its d.c. level by more than 50 mV, 15 samples prior to this time and 184 samples after this time are stored, giving a record length of approximately 64 μs. For each of the four channels, the time at which the signal deviated from d.c., and the maximum (absolute) signal level in the ten following sampling intervals, are recorded.

Several different algorithms are being evaluated to use these arrival times and amplitudes to triangulate the position of the impact and estimate the magnitude of the impact. The most efficient and accurate of these will be optimized and included in one of the processing modules.

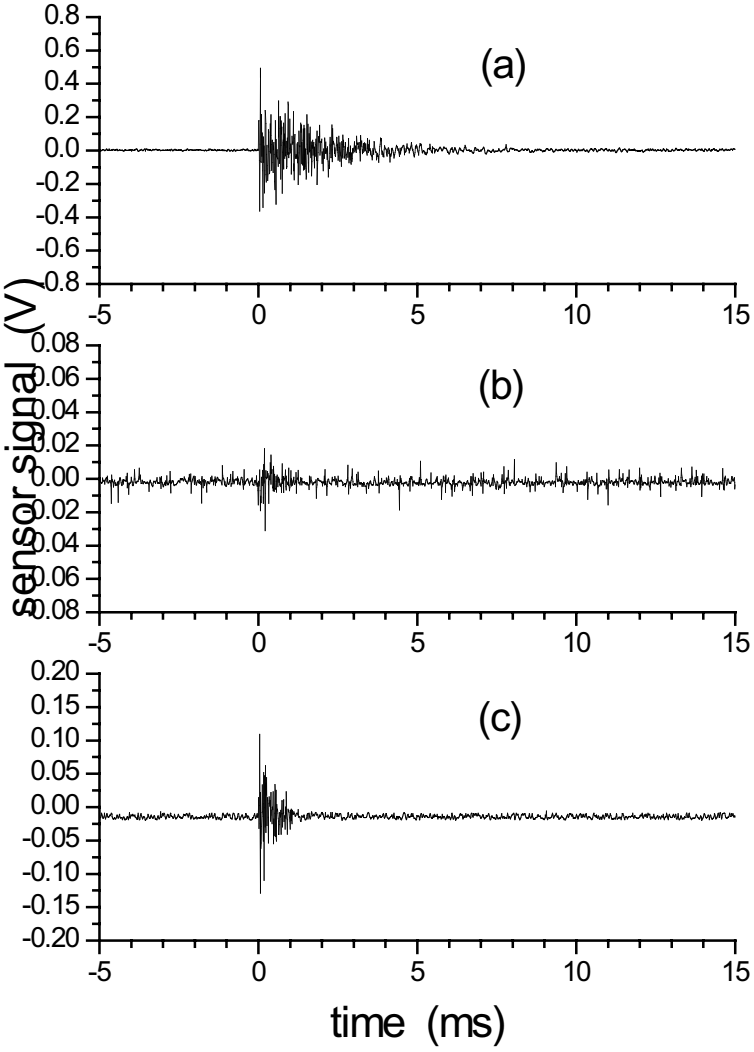

Figure 7: Signal from a small-area sensor monitoring a laser-generated impact, on a longer timescale than Figure 6. (a) Raw signal. (b) Signal after high-pass filtering. (c) Signal after amplification and low-pass filtering. Impact at time t = 0.

4. Architecture and Performance of the Physical Cells

4.1 Introduction

In the System Overview (Section 2) it was explained that cells consist of sensors, a Data Acquisition Sub-module and a Network Application Sub-module, and the architecture and function of these sub-modules are described in this Section. Point-to-point communications links are provided in the Network Application Layer by serial communication links between Network Application Sub-modules, and in this section the communications stack based on these physical links will also be explained.

4.2 Data Acquisition Sub-Module

The Data Acquisition Sub-module (DAS) is connected to the four sensors in the cell, and the purpose of the sub-module is to detect impacts from the signals received from each sensor. For each sensor the amplitude of the signal is measured, and the relative time between impacts on each sensor can be used to determine the location of impacts. This information is then communicated to the attached Network Application Processor.

The analog signals from the sensors are amplified and filtered prior to digitization. It was found the spectral region of most interest lay between 500 kHz and 2 MHz, thus a high pass filter to reject signals below 500 kHz was used, followed by a 5^{th} order Butterworth low-pass filter with the -10 dB frequency at 2 MHz, the latter also being the anti-aliasing filter.

The Texas Instruments TMS320F2810 was selected as the DAS processor (CTIP, 2003). For the initial development stages of the DAS seven development system boards from Spectrum Digital (Stafford, Texas) were used, along with a daughter board that we designed containing the analog electronics, connected to a subset of the Network Application Sub-modules.

4.3 Network Application Sub-Module

The purpose of the Network Application Sub-module (NAS) is to receive information from the attached Data Acquisition Sub-modules (it is possible to have more than one), along with information communicated from other Network Application Sub-modules, to perform the processing that is central to the distributed intelligence of the health monitoring system. The other purpose of the NAS is to provide the network communications: the communications stack will be described in the following sub-section.

Our design for the NAS, which is only 80 mm × 80 mm in size to allow stacking behind the DAS, which in turn will be mounted behind the sensors, is shown in Figure 8, and contains the following main components.

Texas Instruments TMS320VC5509, which is a 288 MIPS fixed-point digital signal processor.
8 Mbytes of volatile memory (SDRAM).
2 Mbytes of non-volatile memory (FLASH).

High-speed synchronous serial communications link to the DAS (using the McBSP built into the DSP). The communications software is implemented using a simple fixed-length packet for the transfer of data.
Four high-speed (maximum 1.5 Mbps) asynchronous serial links for NAL communications using the Texas Instruments TI16C754 quad UART.

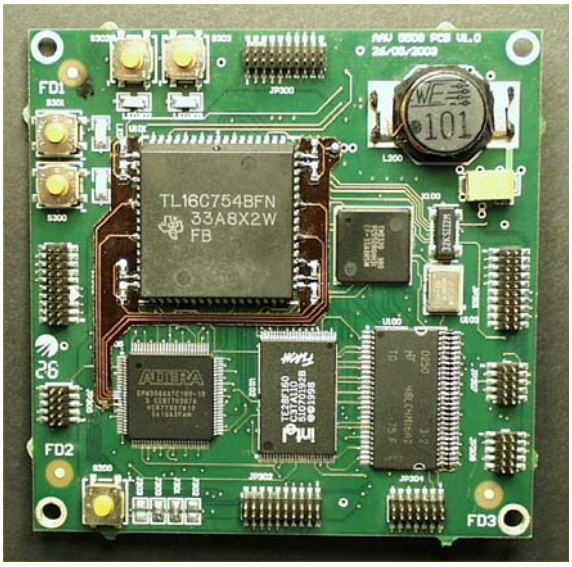

Figure 8: Network Application Sub-module with connections to all four communications ports. The connection to the Data Acquisition Sub-module is on the other side of the PCB.

A network of 16 of these modules has been constructed (see Figure 9), and by March 2004 all 192 of these modules will have been manufactured and integrated into the concept demonstrator. The communications software implemented on these modules is described in the next sub-section, and the agent software providing the distributed processing that runs on these modules is described in Section 6.

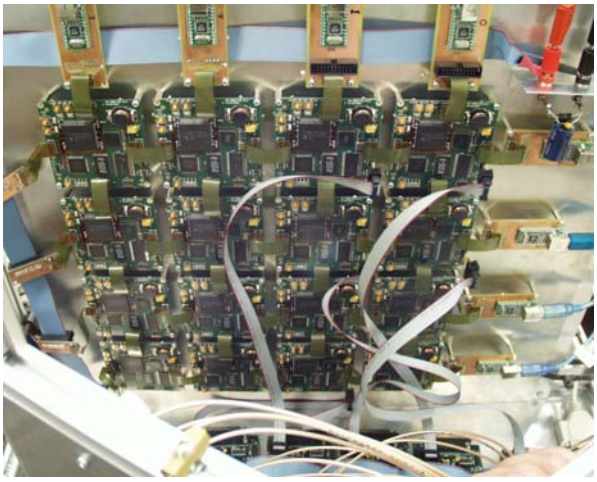

Figure 9: The 4 × 4 array of NAL boards mounted in the Concept Demonstrator frame.

An overall view of the system, including the aluminium panels with sensors attached, the signal conditioning boards, the data acquisition sub-modules, and the network application sub-modules, is shown in Figure 10.

4.4 Network Communications

The network implemented in the Network Application Layer (NAL) is used for a number of purposes, some of which are only for use in the test-bed and would not be present in a deployed IVHM system. The main communication categories are:

> communication between agents (or other processing) running on separate NAL modules to implement the distributed system intelligence and initiate actions,
> distribution of software to network application and data acquisition modules,
> and transmission of diagnostic information for visualizing the status of the test-bed and studying its behavior.

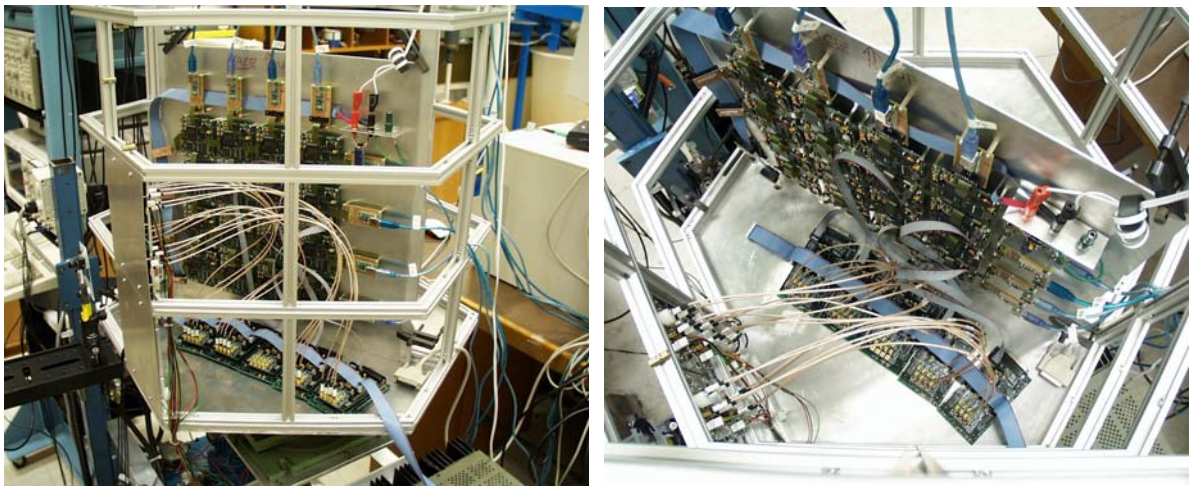

Figure 10: Photographs of the electronic modules mounted in the CD framework. The 2812 DSK boards are the five located on the base of the CD. These are connected via shielded cables to the signal conditioning boards mounted behind the aluminium panel, and via ribbon cable to the Network Application Sub-modules in the 4 × 4 NAL array.

The communications are implemented in a layered manner so that additional functionality can be readily added. At the lowest layer, the communications between processors use asynchronous serial communications, and the data is formatted into packets using a protocol that is a simplification of the Point-to-Point Protocol (PPP) (Simpson, 1994a, 1994b) that is widely used for connections to the internet. This permits multiple network protocols to be used simultaneously on the network. There are currently three network protocols defined, which are described in the following paragraphs.

The Link Control Protocol (LCP) is a special protocol used to control each link. This protocol detects when a processor is connected or disconnected and monitors the status of a connected link. When a connection is detected the LCP at both ends negotiate a serial speed to use. This negotiation is done at a base speed of 9600 bps, and the maximum serial communications rate is 1.5 Mbps.

The Simple Agent Protocol (SAP) is used for the agent-based processing algorithms in each NAS to communicate with another NAS. These agents only communicate with their neighbours, so routing of the packets through the network is not required. For studying the effects of network errors on the agent algorithms we have the ability to simulate random bit errors in SAP packets, where we can control the error probability as a parameterized function of the distance of the cell from an 'impact'.

The Flood Protocol (FP) implements a flooding algorithm, and is used to distribute software to the modules and for modules to send diagnostic and status information back to a test-bed diagnostic computer, which visualizes and analyses the state of the system.

4.5 Measurement of Impact Message Delay

One method of evaluating the performance of the network of physical cells is to measure the time delay of a message that is transmitted around the network. This has been done by routing a message as shown in Figure 11.

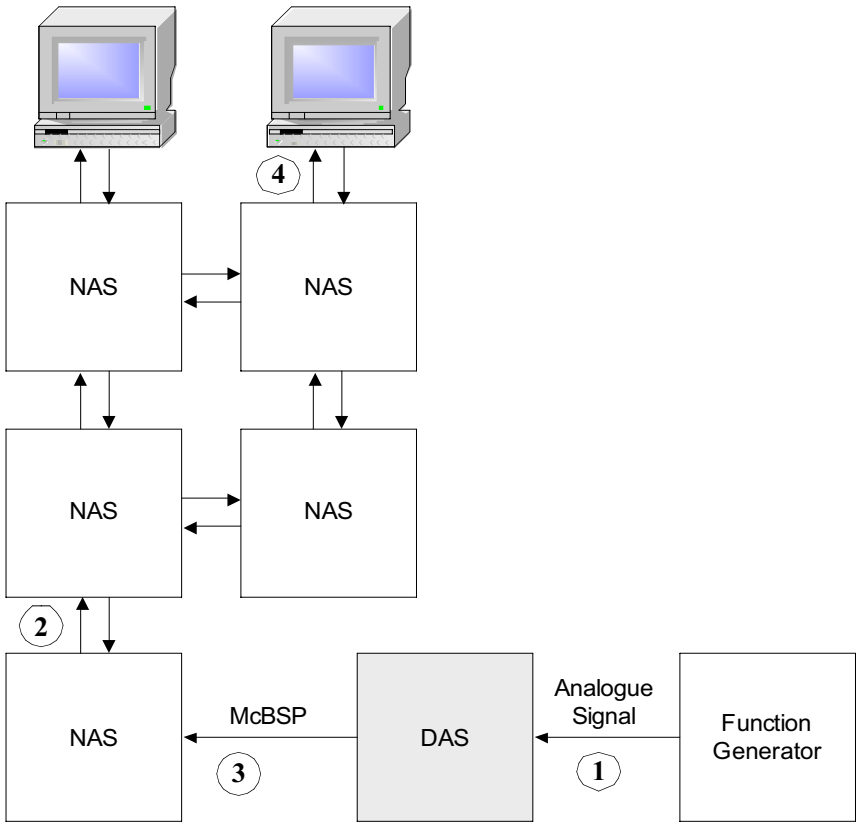

Figure 11: Schematic diagram of the arrangement for measuring impact message delay. The numbers in this figure refer to the monitored channels shown in Figure 12.

A function generator was used to generate pulses, which triggered the data acquisition sub-module (DAS) to report an impact over the McBSP link to a network application sub-module (NAS), which in turn flooded the message through the network. A digital storage oscilloscope was used to examine the numbered signals in the diagram, and two typical results are shown below in Figure 12.

From the screen shots of Figure 12 the following delays can be read. On each screen the four traces, numbered from the bottom of the screen upwards, are signals measured at the correspondingly numbered points in Figure 11. The positive transition on the bottom trace (no.1) represents the simulated impact.

Delay Measurement	**Upper**	**Lower**
Impact to start DAS report on McBSP (Trace 3)	0.75 ms	1.12 ms
Impact to start NAS report (flood) (Trace 2)	1.18 ms	1.58 ms
Impact to reception of report at link distance 3 (Trace 4)	2.40 ms	2.80 ms
Delay per link	0.40 ms	0.40 ms

From these results it can be seen that there is a significant variability in the time the DAS takes to report the impact, and then the message is flooded through the network at a rate of 0.4 ms per link with light network traffic load.

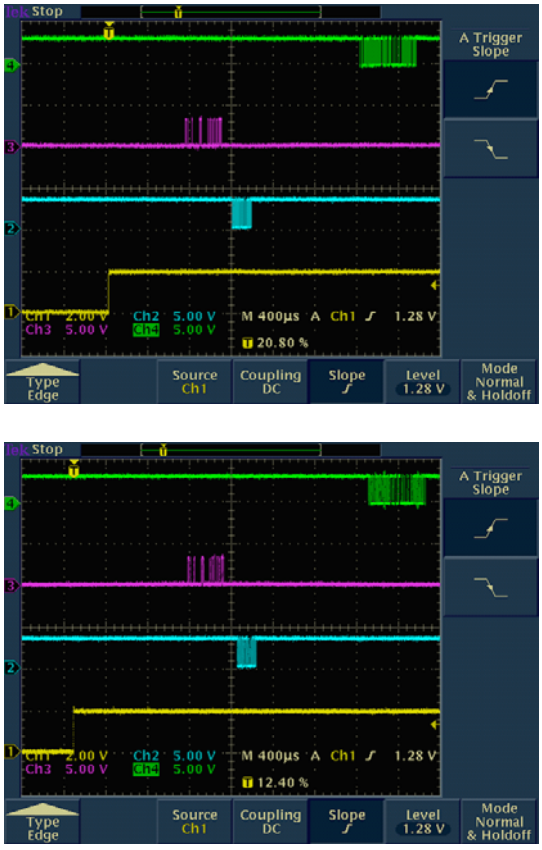

Figure 12: Results of the impact message delay measurement.

4.6 The Simulated Cells

Besides the physical cells described in the previous section, there are also simulated cells to allow the agent-based processing algorithms to be tested in a system larger than that physically implemented. This is particularly important when using multi-agent systems, as the emergent behavior in large systems may be qualitatively different from that in small systems. The cells are simulated on a cluster of Windows XP-based PCs. The Data Acquisition Sub-module is not simulated; rather, a set of pre-programmed events can be triggered using the Graphical User Interface (GUI) with a mouse (see Figure 13). Each PC can simulate multiple cells, with a high-end PC capable of simulating up to 16 cells. There is no limit on the number of PCs that can be connected in the cluster.

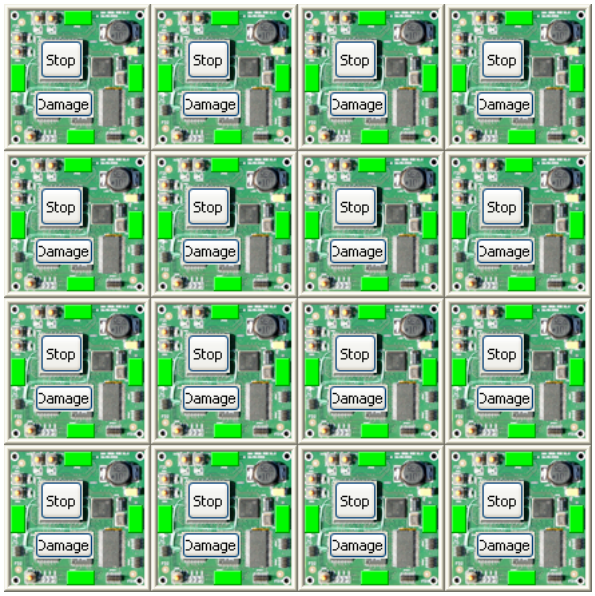

Figure 13: The graphical user interface on a PC simulating a 4 × 4 array of cells.

The connections between hardware and software NAS modules are asynchronous serial communications links using serial modules from Gigatechnology (Southport, Queensland) that allow data rates up to 1.5 Mbps. However, the connection between software NAS modules (whether on the same or different PCs in the cluster) is via UDP running over a 100 Mbps switched ethernet, and for this a separate data link layer, and its associated link control protocol, were implemented. Both data link layers, whether using serial or UDP links, present the same interface to the higher levels of the communication stack, so the type of data link in use is transparent to the other network protocols, and the agent code which communicates via the SAP.

The NAL software consists of the agent code and the communications code, and these have been written so that most of the code is the same on both the hardware cells (running on the TMS3205509 DSP) and on the simulated cells (running on an Intel Pentium 4 processor). This ensures that the same algorithms are implemented on both platforms. The only exceptions to this are interface classes that were implemented to hide the operating system and hardware dependencies from the rest of the software, and the additional use of the UDP

data link on the simulated cells. One issue that has been identified with the simulated cells is that while the physical cells typically respond to packets within a couple of hundred microseconds (as a real-time operating system is running on the DSP hardware), the response time on the simulated cells (using Windows XP) is typically of the order of ten milliseconds. For the present agent algorithms this is not a problem, but it is a reminder that there are significant differences between physical and simulated cells that should not be ignored, and which may potentially lead to differences in the emergent behavior between the two systems.

5. System Management and Visualization

5.1 Introduction

A workstation is used to operate and monitor the test-bed. It is important to make clear that this workstation does not control the operation of the system when the agent software is running: in this case it acts simply as a display system that provides a visual output of the state of each cell.

The system has been designed so that this workstation can control the network functions by being attached either to one of the physical cells (using serial communication) or to one of the simulated cells (using either serial or UDP communication). This functionality is being expanded with further development of the test-bed, and current operations include the following.

Distribution of code to the cells.
Initialization of the clock time on the cells.
Control of the location and error rate of bit corruption of SAP packets for testing agent-based processing algorithms (this was described in the Network Communications section).
Dynamical determination and display of the network topology status of each link (this is seen in Figure 14, where each cell is shown and the link status is color coded), where the addition or removal of cells or links are displayed in real-time.
Display of cells suffering damage, whether due to impacts or other sources of failure (these are shown in red in Figure 14).
Display of agent processing state (described below).

5.2 Visualization software

CDVis is the visualization program developed to allow intuitive analysis of the operation and performance of the AAV concept demonstrator. CDVis can be attached to the cell network at any arbitrary point since it is has been built on the same underlying communication classes used by the cells. The connection can be either through direct serial link to a physical cell's port or through any available UDP port to a simulated cell.

Upon connection to the system, CDVis immediately probes the system to begin dynamically constructing the topology of the system. The process starts by firstly obtaining the immediate neighbouring cell's 64-bit unique identity (UID) through the DataLink layer protocol. This UID is then added to a queue of UIDs to be interrogated.

This queue is progressively processed, generating a "Request Connection Status" (RCS) flood packet for each UID, which is subsequently removed from the queue. The RCS command takes the UID of the targeted cell as a parameter, flooding the request through the system in order to reach the desired cell from which to obtain information. When the designated cell receives the request, it causes the cell to report the connection status from all its four ports. The connection status report consists of whether each port is connected and if so, additionally reports the port speed and the neighbouring UID on that port. When the visualizer receives the report, the cell's status is then known or updated.

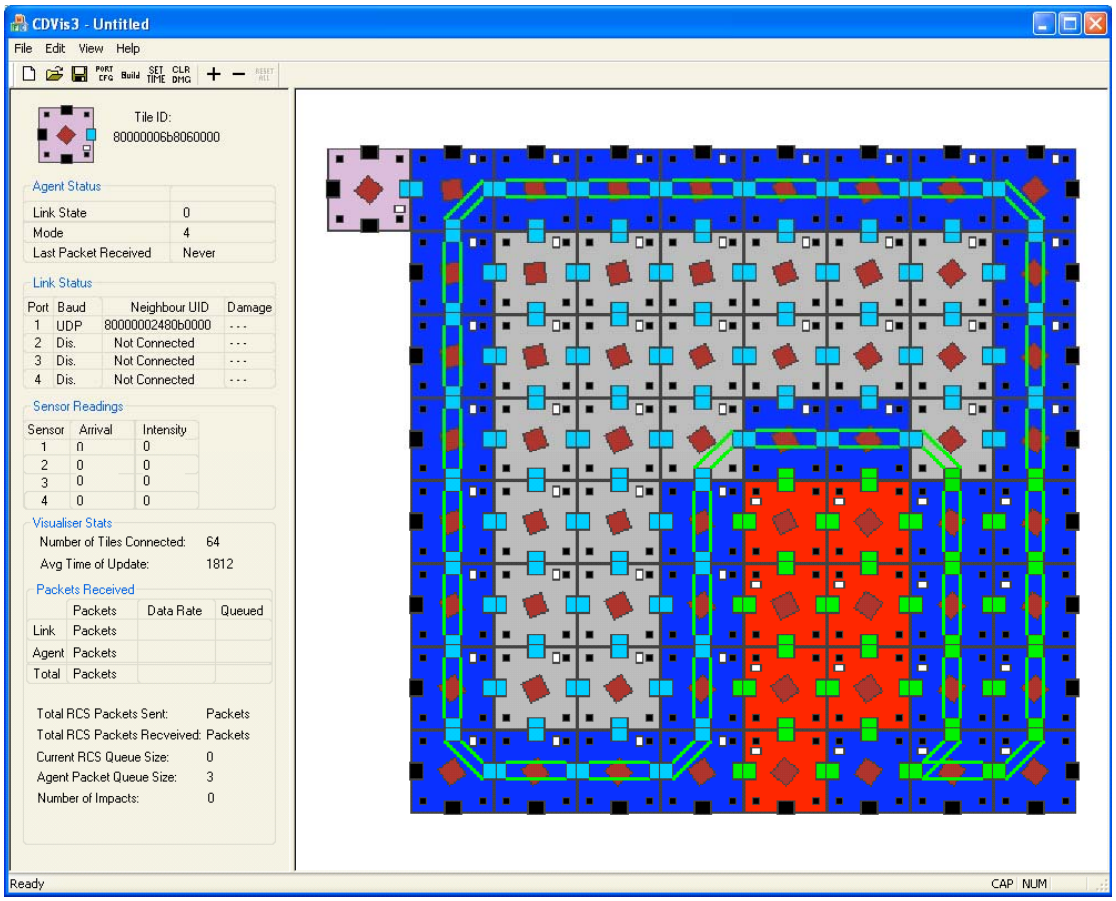

Figure 14: The interface on the system control workstation provides a dynamic display of the network. The cells in red have suffered impact damage, and the blue cells are at a boundary.

Unknown UIDs discovered from RCS reports are added to the queue of cells to be interrogated, which in turn generate additional RCS reports. These reports generate additional unknown UIDs, until eventually all cells and their connectivity have been discovered.

The system has been designed such that when a cell detects any new connection or disconnection, a connections status report is generated. Therefore, if a link between two cells is broken, both cells will generate a connection status report and flood this through all other functioning ports. This functionality is utilized by the visualizer to update the connection status of cells in the event that a new connection or disconnection has occurred. When a disconnection has been detected, the UID of the cell disconnected is placed onto the queue to be interrogated and also on a “time out” queue. If the connection status is not received before the time out period, the cell is classed as not responding and hence removed from the CDVis representation of known cells.
The visualizer not only provides an intuitive visual representation of connectivity of the system, but also provides intuitive feedback on the current state of logic of each cell in the

system. Currently the agent status mode, link state, impact intensity on the sensors, port connection type and speed can be determined from the pictorial representation on the screen. However, selecting a cell of interest with the mouse displays additional details such as the time the last packet was sent from the cell, the link state number, the delay times and impact energy readings of the sensors, and the connection status of the cell including the port speeds and UIDs of neighbouring cells.

CDVis also displays a number of more general details, such as the number of cells connected to the network, the average time between the cells sending the messages and their receipt by the visualizer, the length of the various visualizer queues, communication data rates, and the total number of impact reports.

Useful global functions are also provided to allow the broadcast of visualizer local time throughout the system and broadcasting of the “Clear Damage” command that reverses the corruption of the agent communications caused by the simulated damage profile.

Currently the visualizer is being extended to allow both targeted and *en mass* starting and stopping of the agent logic from the visualizer.

6. Intelligent Distributed Processing

6.1 Introduction

The solution that has been adopted for the problems of handling the vast quantities of data and making the IVHM system robust, is to distribute the processing so that most computation takes place near the data source, and there is no single or small number of points of failure resulting from the use of central computers. In other words, without centralized controllers, agents (cells) are expected to self-organize and survive on the basis of local, rather than global, information (no single agent has access to information about any others but its neighbours). This approach uses the idea of localized algorithms, in which simple local node behaviours achieve a desired global objective, while communicating only with nodes within an immediate neighbourhood.

Our proposed approach to self-organizing multi-agent networks is based on an iterative process including the following steps:

a) forward simulation leading to emergent behaviour for a class of localized algorithms;
b) quantitative measurement of spatio-temporal stability of the emerging patterns, using information-theoretic metrics for phase transitions; and
c) evolutionary modelling of the algorithms, with the fitness functions corresponding to the metrics obtained at step b).

6.2 Impact boundaries

The first agent task that has been implemented for the concept demonstrator is to trace *impact boundaries* and their spread despite connectivity disruptions and cell failures – analogous to staged repair in biological systems. Impact boundaries enclose critically damaged areas, and it is desirable that such boundaries quickly form continuously-connected closed circuits, which are robust to fluctuations caused by proximity to the impact. Our initial work has lead to the formation of a boundary that is well placed in separating the cells that suffered unrecoverable communication damage (including those that were completely destroyed) from the cells that are able to communicate to their normal functional capacity. The algorithm enables self-organization of the internal "scaffolding", the "membrane", and the "frame" of the desired closed boundary regardless of cell shape (triangular or square). An example of this is shown in Figure 15, where red cells form the scaffolding, yellow cells form the membrane and blue cells form the frame, and the underlying boundary is shown with white links. However, on some occasions the boundary is erratic and unstable: some cells frequently change their states from "frame" to "scaffolding" to "normal", etc. The reason for this spatial and temporal instability is that a simple detection of a missed acknowledgement may sometimes be insufficient to determine a cell's state (to provide stability), especially when the cells involved are on the periphery of the damaged area. In other words, in order to detect a persistent failure in communications with an adjacent cell, the cell needs to filter away spurious occasional miscommunications.

The length ρ of such a filter (i.e., the cell-to-cell communication history, which is kept by each cell), is an important parameter, directly affecting spatial and temporal stability of self-organizing impact boundaries. Our experiments characterized the dynamics of multi-

cellular impact boundaries in terms of generic information-theoretic properties, such as the Shannon entropy, and verified that larger values of ρ lead to stable boundaries. In particular, the developed quantitative information-theoretic metrics clearly identify phase transitions, separating chaotic dynamics from ordered and robust patterns.

These techniques have also been used in our experiments on evolutionary modelling of agent properties. Here we incorporate the stability metrics within fitness functions of genetic algorithms, and evolve parameters such as the communication history ρ, to achieve the desired global behavior. The results have shown that a phase transition exists between $\rho = 4$ and $\rho = 5$, and the latter critical value ensures stability.

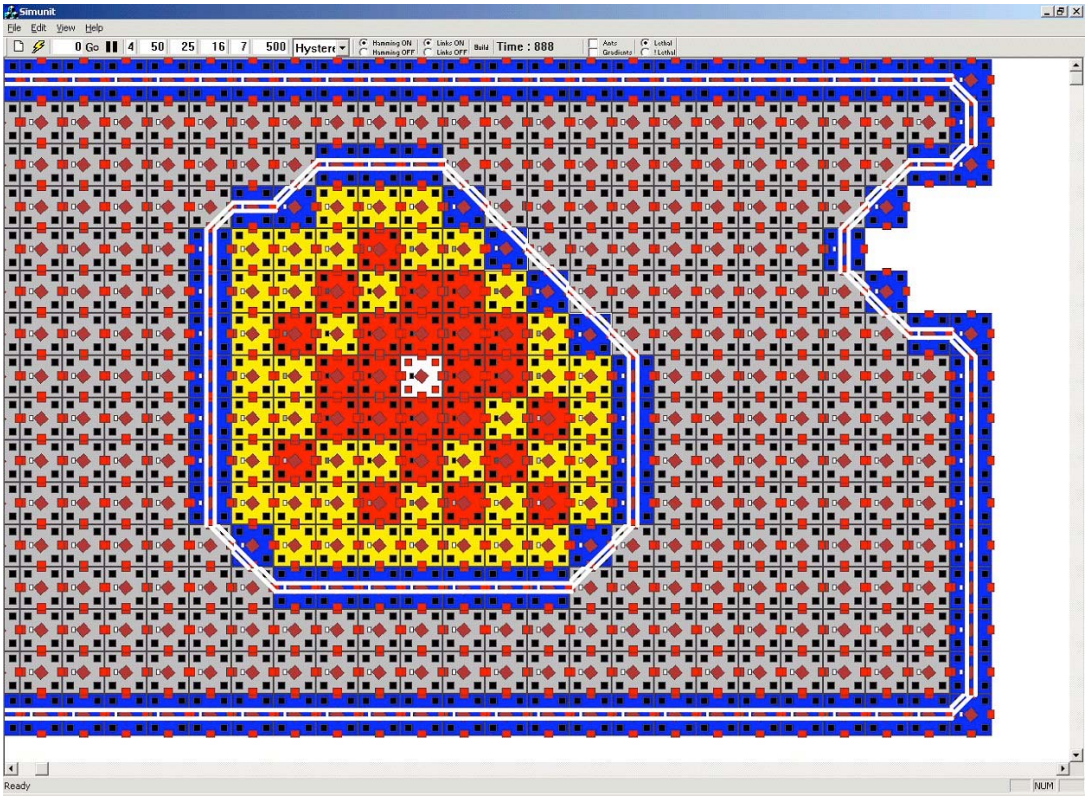

Figure 15: Software simulation of self-organized impact boundary formation.

6.3 Recovery Membranes

As an emergent structure, the impact-surrounding region has unique higher-order properties, such as having an *inside* and an *outside* and, importantly, a *recovery* property.

To support these conjectures, we differentiated between the cells that shut down (switch to the "silent mode") because either they have no incoming "OK" messages (the first type), or they receive no "Acknowledgement" message from any neighbour cell (the second type).

Figure 15 highlights the differences: the first type is shown with red colour, while the second type is shown in yellow. It is quite obvious that the latter kind forms a "membrane" separating proper scaffolding from the frame boundary. It is precisely due to this membrane that the resulting impact boundary is stable: without it, the cells on the closed boundary (blue cells) would be confused by intermittent messages from scaffolding cells (red).

The membrane always forms on the inside of the closed boundary, and on the outside of the scaffolding. Importantly, membrane forms within the impact-surrounding region, providing a clear indication of the cells that are inside and the cells that are outside the boundary. Interestingly, unlike the scaffolding and the frame boundary (double-linked white cells in Figure 15), the membrane was not a designated state into which a cell can switch.

Since both kinds of cells (scaffolding and membrane cells) go into "silent mode", the behaviour may be extended with the following: if the cell state is in a **scaffolding** state and there are no mis-communicating neighbours, or if there are no communicating neighbours, switch the cell to the **recovery** state and resume sending messages.

This behaviour enables totally isolated cells to be in a state ready to be repaired (recovery state), a feature that may be needed when a repair is in progress and cells are being transported across a panel. If a repair is initiated and a healthy cell replaces a scaffolding cell (including one in the membrane), then the recovery mode results in shrinking membranes and impact-surrounding regions. Figure 15 shows a scenario in which seven healthy cells were removed from the right edge of the panel and used to replace seven damaged cells in the top-right corner of the impact-surrounding region. This repair action was not initiated by the system itself at this stage. The fourteen cells involved were manually transported from and to the damaged corner. This was done only to illustrate the recovery mode and the potential for self-repair.

6.4 Impact networks

Impact boundaries emerge as a result of local and short-range interactions. However, sometimes it is necessary to acquire data from remote cells. An *impact network* connecting cells that registered non-critical impacts is a good example of this process. When dealing with non-critical impacts, there is a possibility to extract information directly from the cells that register the impact. Moreover, in these scenarios the communication links even between the cells that are close to the impact point are likely to remain intact. This suggests the use of the impact points (detected by the individual cells) as nodes in the impact network (a cluster or a minimum spanning tree) in order to facilitate fast inspections of impact areas, identification of high densities of impacts (e.g. a meteor shower), and routing of repair resources.

The concept of the impact network makes it possible to apply some of the fairly well-known algorithms, such as Ant Colony Systems (ACS) algorithms to the problem of impact analysis in the AAV. The ACS algorithms use the ability of agents to indirectly interact through changes in their environment (*stigmergy*) by depositing pheromones and forming a pheromone trail. They also employ a form of *autocatalytic behaviour*: the probability with which an ant chooses a trail increases with the number of ants that chose the same path in the past. The process is thus characterized by a positive feedback loop.

The most interesting aspect of this autocatalytic process, verified in our experiments, is that finding the shortest path around an obstacle is an emergent property of the interaction between the obstacle shape and the ants' distributed behaviour. Figure 16 shows white cells that detected damage and different shades of green (dark) represent the trail intensity – the lighter the colour the more intense the pheromone track. The analysis of spatial stability of impact networks used two critical parameters: evaporation (retention) rate λ and the ants' generation interval **T**. The retention rate λ determines how much pheromone remains in the cell at the end of each cycle ($\lambda = 1.0$ means that there is no evaporation), and **T** sets the interval for generating new ants by every affected cell – more precisely, every cell generated four ants for each interval **T**. The modelling experiments have shown that robust trails emerge for low generation intervals and high retention rates, in particular for $\mathbf{T} = 20$ and $\lambda = 0.98$.

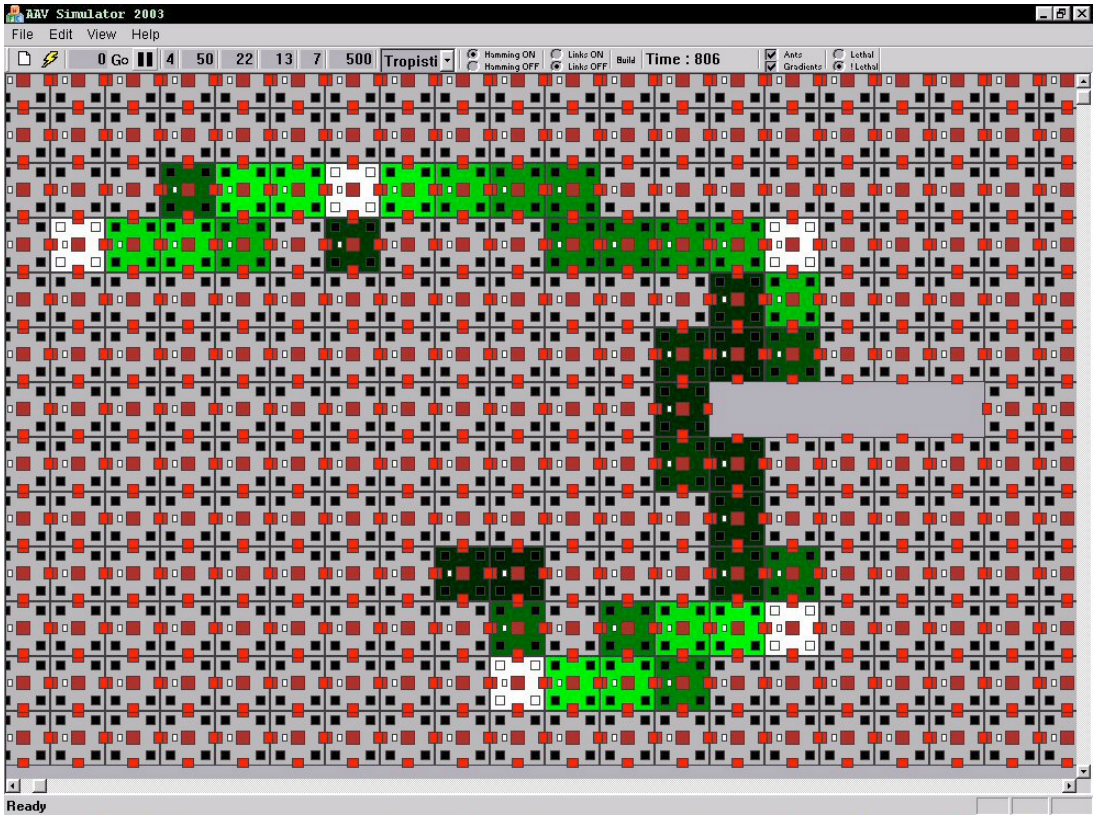

Figure 16: Software simulation of an impact network joining five impact sites.

7. Summary and Conclusions

This Report describes the first phase of the implementation of the Concept Demonstrator/Experimental Test-bed system containing sensors and processing hardware distributed throughout the structure, which uses multi-agent algorithms to characterize impacts and determine an appropriate response to these impacts. The system is divided into cells, each of which contains four acoustic emission sensors and two digital signal processors, and serial communication is provided between the cells. For testing the agent algorithms the system can be expanded by the inclusion of simulated cells.

The present status of the system is that 16 physical cells have been constructed, although only five of these presently contain the sensors and associated data-acquisition sub-modules. There will be 192 physical cells in the final system, which is due for completion in March 2004. The communications stack has been fully implemented and tested on all systems. The software modules for simulating cells and managing the test-bed are fully operational, although additional functionality will be added over time.

While we have successfully implemented distributed processing algorithms using a multi-agent system approach, further functionality will be required to fully characterize and respond to impacts. This system is a powerful and flexible experimental platform for developing sensors, communications systems and multi-agent based algorithms for an intelligent vehicle health monitoring system for deployment in space vehicles.

Acknowledgements

The assistance of Prof. Richard Morgan, Prof. Ray Stalker and Matt Clark of the Centre for Hypersonics, University of Queensland, in obtaining the high-velocity particle impact data is gratefully acknowledged.

References

CTIP (2001). *Development and Evaluation of Sensor Concepts for Ageless Aerospace Vehicles*, Report 1. CSIRO Telecommunications and Industrial Physics. Report No. TIPP 1516, 2001. Also published as NASA Technical Report no. NASA/CR-2002-211772.

CTIP (2002). *Development and Evaluation of Sensor Concepts for Ageless Aerospace Vehicles. Development of Concepts for an Intelligent Sensing System.* Report 2. CSIRO Telecommunications and Industrial Physics. Report No. TIPP 1517, May 2002. Also published as NASA technical report NASA/CR-2002-211773.

CTIP (2003). *Development and Evaluation of Sensor Concepts for Ageless Aerospace Vehicles. Report 3: Design of the Concept Demonstrator.* CSIRO Telecommunications and Industrial Physics. Report No. TIPP 1628, January 2003. Also NASA/CR-2008-215307.

Hedley, M., Johnson, M., Lewis, C., Carpenter, D., Lovatt, H., Price, D. C., (2003). "Smart Sensor Network for Space Vehicle Monitoring". In Proceedings of the International Signal Processing Conference, Dallas, Texas, March 2003.

Simpson, W., (1994a). "The Point-to-Point Protocol (PPP)", RFC1661, http://www.faqs.org/rfcs/rfc1661.html.

Simpson, W., (1994b). "PPP in HDLC-like Framing", RFC1662, http://www.faqs.org/rfcs/rfc1662.html.

REPORT DOCUMENTATION PAGE

Form Approved
OMB No. 0704-0188

The public reporting burden for this collection of information is estimated to average 1 hour per response, including the time for reviewing instructions, searching existing data sources, gathering and maintaining the data needed, and completing and reviewing the collection of information. Send comments regarding this burden estimate or any other aspect of this collection of information, including suggestions for reducing this burden, to Department of Defense, Washington Headquarters Services, Directorate for Information Operations and Reports (0704-0188), 1215 Jefferson Davis Highway, Suite 1204, Arlington, VA 22202-4302. Respondents should be aware that notwithstanding any other provision of law, no person shall be subject to any penalty for failing to comply with a collection of information if it does not display a currently valid OMB control number.
PLEASE DO NOT RETURN YOUR FORM TO THE ABOVE ADDRESS.

1. REPORT DATE *(DD-MM-YYYY)*	2. REPORT TYPE	3. DATES COVERED *(From - To)*
01- 11 - 2008	Contractor Report	

4. TITLE AND SUBTITLE

Development and Evaluation of Sensor Concepts for Ageless Aerospace Vehicles: Report 4 – Phase 1 Implementation of the Concept Demonstrator

5a. CONTRACT NUMBER

5b. GRANT NUMBER

5c. PROGRAM ELEMENT NUMBER

6. AUTHOR(S)

Abbott, David; Batten, Adam; Carpenter, David; Dunlop, John; Edwards, Graeme; Farmer, Tony; Gaffney, Bruce; Hedley, Mark; Hoschke, Nigel; Isaacs, Peter; Johnson, Mark; Lewis, Chris; Murdoch, Alex; Poulton, Geoff; Price, Don; Prokopenko, Mikhail; Rees, David; Scott, Andrew; Seneviratne, Sarath; Valencia, Philip; Wang, Peter; Whitnall, Denis

5d. PROJECT NUMBER

PO L-71346D

5e. TASK NUMBER

5f. WORK UNIT NUMBER

7. PERFORMING ORGANIZATION NAME(S) AND ADDRESS(ES)

NASA Langley Research Center
Hampton, VA 23681-2199

8. PERFORMING ORGANIZATION REPORT NUMBER

Report No. TIPP 1898

9. SPONSORING/MONITORING AGENCY NAME(S) AND ADDRESS(ES)

National Aeronautics and Space Administration
Washington, DC 20546-0001

10. SPONSOR/MONITOR'S ACRONYM(S)

NASA

11. SPONSOR/MONITOR'S REPORT NUMBER(S)

NASA/CR-2008-215542

12. DISTRIBUTION/AVAILABILITY STATEMENT

Unclassified - Unlimited
Subject Category 38
Availability: NASA CASI (301) 621-0390

13. SUPPLEMENTARY NOTES

Langley Technical Monitor: Edward R. Generazio

14. ABSTRACT

This report describes the first phase of the implementation of the Concept Demonstrator. The Concept Demonstrator system is a powerful and flexible experimental test-bed platform for developing sensors, communications systems, and multi-agent based algorithms for an intelligent vehicle health monitoring system for deployment in aerospace vehicles. The Concept Demonstrator contains sensors and processing hardware distributed throughout the structure, and uses multi-agent algorithms to characterize impacts and determine an appropriate response to these impacts.

15. SUBJECT TERMS

IVHM; NDE; NDI; NDT; Nondestructive evaluation; Smart structures; Vehicle heath monitoring

16. SECURITY CLASSIFICATION OF:			17. LIMITATION OF ABSTRACT	18. NUMBER OF PAGES	19a. NAME OF RESPONSIBLE PERSON
a. REPORT	b. ABSTRACT	c. THIS PAGE			STI Help Desk (email: help@sti.nasa.gov)
					19b. TELEPHONE NUMBER *(Include area code)*
U	U	U	UU	36	(301) 621-0390